The Stability Transition from Stable to Unstable Frictional Slip with Finite Pore Pressure

Raphael Affinito[1], Clay Wood[2], samson marty[3], Elsworth Derek[1], and Chris Marone[4]

[1]The Pennsylvania State University
[2]Penn State University
[3]Rock and Sediment mechanics laboratory - PSU
[4]Pennsylvania State University

March 16, 2023

Abstract

Pore fluids are ubiquitous throughout the lithosphere and are commonly cited as the cause of slow-slip and complex modes of tectonic faulting. We investigate the role of fluids for slow-slip and the frictional stability transition and find that the mode of fault slip is mainly unaffected by pore pressures. We shear samples at effective normal stress (σ'n) of 20 MPa and pore pressures Pp from 1 to 4 MPa. The lab fault zones are 3 mm thick and composed of quartz powder with median grain size of 10 μm. Fault permeability evolves from 10-17 to 10-19 m2 over shear strains up to 26. Under these conditions, dilatancy strengthening is minimal. Slow slip may arise from dilatancy strengthening at higher fluid pressures but for the conditions of our experiments slip rate-dependent changes in the critical rate of frictional weakening are sufficient to explain slow-slip and the stability transition to dynamic rupture.

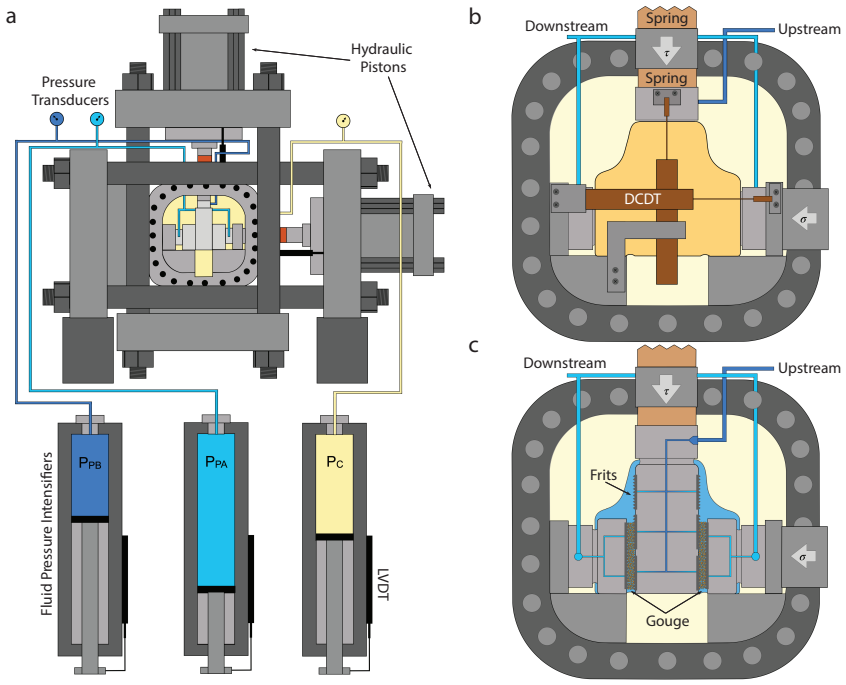

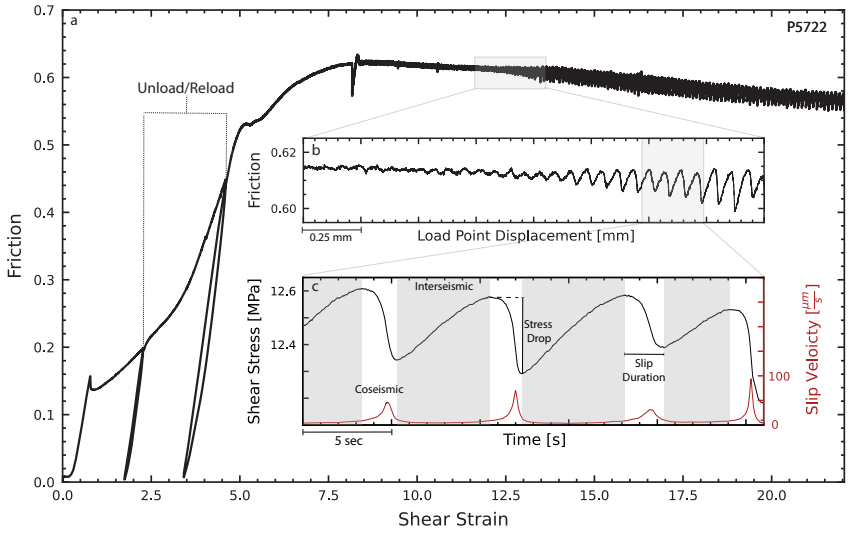

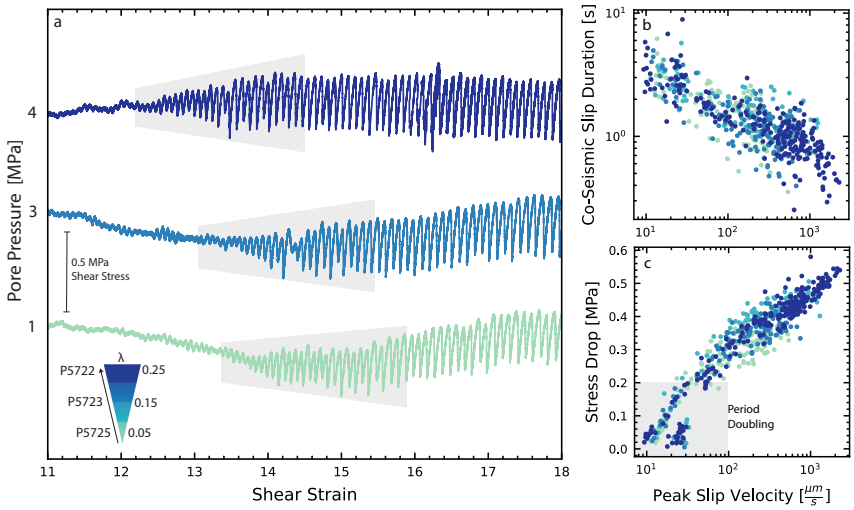

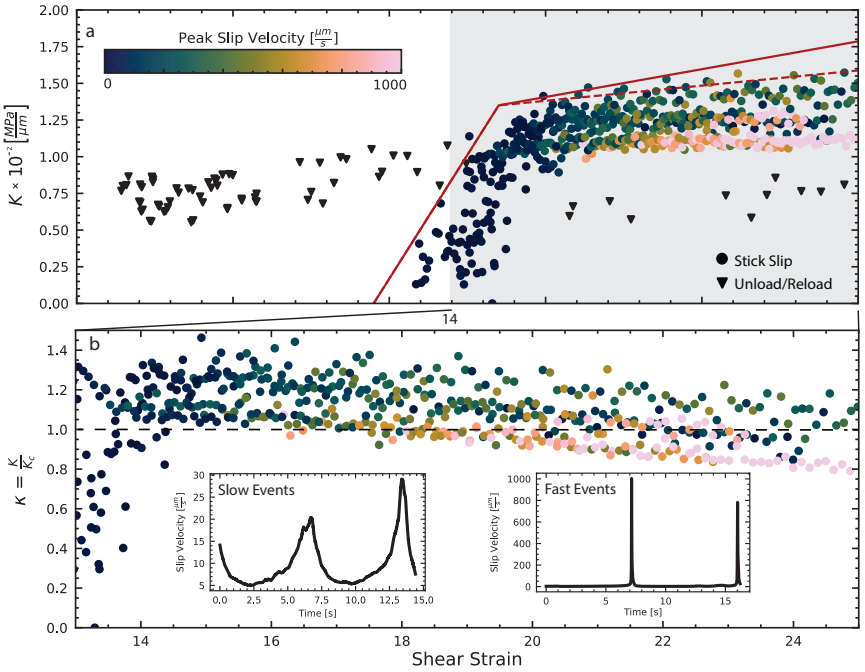

The Stability Transition from Stable to Unstable Frictional Slip with Finite Pore Pressure

R. Affinito[1], C. Wood[1], S. Marty[1], D. Elsworth[1,2], C. Marone[1,3]

[1]Department of Geosciences, Pennsylvania State University
[2]Department of Energy and Mineral Engineering, EMS Energy Institute, and G3 Center, Pennsylvania State University
[3]Dipartimento di Scienze della Terra, La Sapienza Università di Roma
[1]Department of Geosciences, 503 Deike Building, University Park, PA 16802 USA
[2]EMS Energy Institute, Penn State University, C-211 Coal Utilization Laboratory, University Park, PA 16802 USA
[3]Department of Earth Sciences, La Sapienza University of Rome, P.le Aldo Moro, 5 - 00185 Rome, Italy

Key Points:

- Slow-slip events and the transition to dynamic stick-slip failure can occur for fluid-saturated faults.
- For granular fault zones sheared at low pore pressures, the frictional stability transition does not require dilatant hardening.
- Slow earthquakes and quasi-dynamic fault slip modes can be explained by strain rate dependence of the critical frictional weakening.

Corresponding author: Raphael Affinito, affinito@psu.edu

Abstract

Pore fluids are ubiquitous throughout the lithosphere and are commonly cited as the cause of slow-slip and complex modes of tectonic faulting. We investigate the role of fluids for slow-slip and the frictional stability transition and find that the mode of fault slip is mainly unaffected by pore pressures. We shear samples at effective normal stress (σ'_n) of 20 MPa and pore pressures P_p from 1 to 4 MPa. The lab fault zones are 3 mm thick and composed of quartz powder with median grain size of 10 µm. Fault permeability evolves from 10^{-17} to 10^{-19} m^2 over shear strains up to 26. Under these conditions, dilatancy strengthening is minimal. Slow slip may arise from dilatancy strengthening at higher fluid pressures but for the conditions of our experiments slip rate-dependent changes in the critical rate of frictional weakening are sufficient to explain slow-slip and the stability transition to dynamic rupture.

Plain Language Summary

Earthquakes begin and propagate within the fluid-saturated rocks of Earth's crust. Many investigators have suggested that high pore fluid pressure (Pp) is essential for slow earthquakes and tremor. These studies rely on the idea that changes in Pp can impact rupture propagation speed by dilatant volume increase during faulting with concurrent increases in fault normal stress. Thus, understanding the processes that produce slow-slip vs. dynamically propagating rupture is integral to seismic hazard forecasting. Here, we describe experiments on granular faults that produce the full spectrum of slip observed in nature. We measure the mechanical and hydraulic behavior of the faults and determine that frictional and fluid-driven processes occur in conjunction. Importantly, we demonstrate that frictional processes are sufficient to explain slow-slip and the transition to dynamic events without requiring Pp changes.

1 Introduction

Slow earthquakes and other quasi-dynamic modes of fault slip appear to be analogs of ordinary, elastodynamic earthquakes (Dal Zilio et al., 2020). Still, the mechanisms that dictate rupture propagation speed for slow events are poorly understood. In many cases, slow earthquakes occur at depths associated with metamorphic dehydration (Behr & Bürgmann, 2021) and alterations in permeable pathways (Williams, 2019), thus elevated pore pressure is commonly suggested as their cause (Condit & French, 2022). Additionally, laboratory studies have shown that rock fracture and fault slip can induce dilatancy and cause pore pressure to drop and faults to strengthen (Brantut, 2020). These observations are consistent with mechanisms such as seismic pumping, fault-valve behavior (Sibson, 1986), and dilational strengthening (Segall et al., 2010). However, it is often unclear whether dynamic fluid responses act to stabilize fault slip or destabilize via mechanisms such as thermal pressurization (Segall & Rice, 2006). Thus, details of slip-induced volume changes and fault permeability are essential to resolve these issues, yet poorly constrained.

From a frictional perspective, high pore pressure reduces fault strength, bringing it closer to failure (Hubbert & Rubey, 1959; Ellsworth, 2013). However, while the Coulomb-Mohr failure criterion predicts the stress state, it does not address the stability of frictional motion and whether slip will be seismic or aseismic. This is determined by fracture energy considerations and fluid-fault interactions such as storage capacity and fluid diffusion time (Biot, 1941). Thus, while fluids are clearly important, the wide range of conditions under which slow earthquakes occur (Sacks et al., 1978; Bürgmann, 2018) suggests that other mechanisms may play a role.

With the recognition that pore fluid pressures and their pathways are highly variable along subducting interfaces (Behr & Bürgmann, 2021), it may be appropriate to focus on whether changes in pore pressure result in modulation in the effective normal stress or are dissipated by fluid diffusion (Faulkner & Rutter, 2001). Dilational strengthening requires that increased pore volume *via* slip reduces the pore fluid pressure and thus temporarily increases the effective stress across the fault. The resultant change in stress effectively clamps the interface and arrests slip. Thus, it is often assumed as a potential mechanism for SSEs. Yet, the opposite mechanism can also occur, whereby undrained compaction leads to slip *via* fluid pressurization and fault weakening (Segall et al., 2010).

Experimental studies on fracture of intact samples show that dilatancy can stabilizes slip events (Aben & Brantut, 2021). Moreover, measurements of volumetric changes in experimental faults (Marone et al., 1990; Samuelson et al., 2009; Proctor et al., 2020; Brantut, 2020; Aben & Brantut, 2021; Ji et al., 2022) highlight the importance of the drainage state on fluid pressure responses and show that dilatancy rate with fault slip can increase with slip velocity, which could lead to dilatancy hardening. Yet, only a few studies have successfully measured fault zone storage (Wibberley, 2002), as fault zone thickness varies greatly during slip events (Rice, 2006). These data are critical for characterizing the role of dilational processes on slip.

The purpose of this paper is to describe lab work investigating slow slip and the friction stability transition under fluid saturated conditions. Our work builds on observations of slow and complex slip (Scholz et al., 1972; Brantut et al., 2011) and studies demonstrating that complex modes of fault slip can occur when the loading stiffness K is nearly equal to the critical frictional weakening rate (or rheological stiffness) K_c (Gu et al., 1984). Laboratory studies (Leeman et al., 2016) have shown that the full spectrum of fault slip modes can occur when the loading stiffness (K) is nearly equal to the critical weakening rate, $K_c = (b-a)/D_c$, where $(b-a)$ is the friction rate parameter and D_c is the critical friction distance (Gu et al., 1984; Dieterich, 1979; Marone, 1998; Ruina, 1983). Here, we build on an extensive set of works (Leeman et al., 2015, 2016; Scuderi et al., 2016, 2017; Shreedharan et al., 2020) that document the transition from stable to unstable frictional sliding. We show that for the conditions of our experiments

pore pressure has a minor effect on the frictional stability transition and is not the cause of slow slip.

2 Experimental Methods

Our experiments were conducted in a true-triaxial pressure vessel (Figure 1A), using the double direct shear (DDS) configuration (Samuelson et al., 2009; Ikari et al., 2009; Kenigsberg et al., 2020). We used a synthetic fault gouge composed of quartz powder (Min-U-Sil 40) with a median grain size of 10.5 µm. Two uniform layers were constructed using a leveling jig to achieve a reproducible initial thickness of 3 mm. We weighed the layers for each experiment and ensured <10% variability between experiments (see Supplement Table 1). The layers were each 5.7 cm × 5.4 cm in area. For simplicity, we reference all stresses, strains, and displacements to a single fault layer of the DDS arrangement. Total shear displacements ranged from 22 –25 mm, corresponding to shear strain between 20 –26. Samples were sealed in a flexible latex jacket to separate confining and pore pressures (Figure 1C).

Normal stress (σ_n) and shear stress (τ) are applied and maintained *via* servo-controlled hydraulic rams (Figure 1A). Upstream and downstream pore fluid pressures (P_p) and confining pressure (P_c) were independently servo-controlled. For our sample geometry (Figure 1C) fault normal stress is given by σ_n+0.63P_c, for a Terzhagi effective normal stress, $\sigma_n' = \sigma_n + 0.63P_c - P_p$.

P_p is servo-controlled at a constant value and we measure both upstream and downstream volume fluxes to determine fault perpendicular permeability. τ on the fault is applied by advancing the central forcing block of the DDS arrangement at a constant displacement rate. Both normal and shear loads are measured by load cells with a precision of 5 N (Figure 1A). Fault shear and normal displacements are measured with DCDTs external to the pressure vessel and in a few cases with DCDTs internal to the vessel; in all cases, the resolution is ± 0.1 µm (Figure 1B).

Samples were sheared with finite pore pressures between 1 and 4 MPa at 10 µm/s, and thus under fluid-saturated and drained conditions. The pore fluid of de-ionized and de-aired water was delivered to the faults *via* sintered metal frits (Figure 1B). The frits are serrated with saw-tooth faces to ensure coupling to the gouge layer. P_p was monitored using pressure transducers external to the pressure vessel (Figure 1A) with 0.007 MPa resolution. Loads and displacements were recorded continuously at 10 kHz sampling rates and averaged for storage from 1 Hz to 1 kHz, depending on the shear rate.

2.1 Sample preparation

The faults are sealed with a composite latex rubber membrane to isolate P_c from P_p. The seal consisted of three layers to prevent puncture during shear: (1) a 3.2 mm thick latex rubber sheet wrapped around the lower part of the sample, (2) a 0.9 mm thick latex rubber tube, and (3) a 1.5 mm thick dip-molded latex jacket for the DDS configuration (Figure 1C).

2.2 Reduction of apparatus loading stiffness

Our goal is to study the transition from stable to unstable sliding, thus we reduced the shear loading stiffness K to match the critical weakening rate K_c. Stiffness was reduced using two acrylic rods 42-mm in diameter and 35-mm in length in the shear loading column. One rod was outside the vessel at the load point and the other was inside the pressure vessel between the piston and the sample (Figure 1C). Loading stiffness calibration experiments showed that P_c has a negligible effect on the spring stiffness (see Supplementary Figure 1).

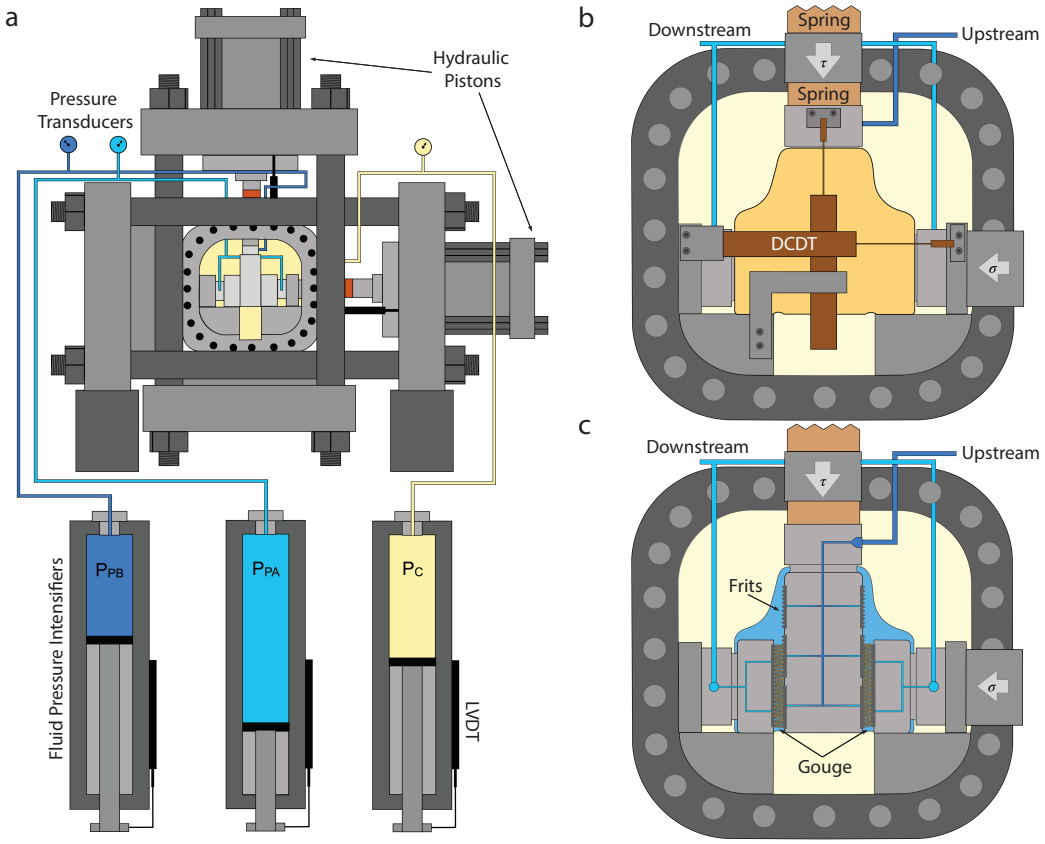

Figure 1. Schematic of the biaxial deformation apparatus and pressure vessel for true triaxial loading. (A) Two hydraulic rams apply normal and shear loads to the double direct shear (DDS) sample. Fluid intensifiers provide upstream and downstream P_p and P_c. (B) Internal DCDTs to measure fault shear and normal displacements. Two springs are placed in series with the vertical loading column to reduce stiffness. (C) We measured fault normal permeability by flowing from the central block to the side blocks of the DDS arrangement. Pore fluids enter the fault via sintered metal frits (Mott Corp.).

2.3 Permeability and fault zone strain

Permeability was measured every 5 mm of shear displacement with the following protocol. (1) While shearing, a constant P_p boundary condition was imposed between the upstream (PpA) and downstream (PpB) (Figure 1A). (2) The vertical piston was locked in place. (3) A 0.5 MPa P_p was imposed from PpA to PpB until the flow rates equilabrated and permeability was measured. This protocol was repeated several times throughout shear. The across-fault permeability was calculated using Darcy's law:

$$k = \frac{Q\mu L}{A\Delta P} \tag{1}$$

Steady-state flow was ensured by measuring upstream and downstream volume flux, where Q is the fluid discharge, μ is the water viscosity at room temperature (24°C), L is the fault layer thickness (accounting for layer compaction/dilation), A is the sample cross-sectional area, and ΔP is the pore pressure differential. Upstream and downstream values of Q differing by <5% were considered steady-state.

2.4 Experimental procedure

Experiments began by applying σ_n of 3 MPa, followed by 2 MPa P_c, after which P_p was increased to 1 MPa. Samples were saturated by (i) bleeding air from pressure lines and (ii) imposing a 0.5 MPa P_p differential across the sample to atmosphere. When constant fluid flow was achieved, (iii) P_p was increased to 1 MPa, and the bleed valve was closed. At this point, upstream and downstream P_p values were equalized, followed by final check for trapped air.

After saturation, σ_n was increased to the target stress (18 –21 MPa) and P_c was increased to 5 MPa. During this compaction stage, P_P was increased to the target value (1 –4 MPa). Experiments began with a permeability measurement, after compaction, followed by a 10 $\mu m/s$ shear loading segment with a shear unload/reload stage at 3 and 6 mm to promote comminution and steady-state shear fabric (Figure 3A). We sheared samples for up to 25 mm, and then locked the vertical piston and made a final permeability measurement (Figure 1B).

3 Results

Stress-displacement curves for our experiments show a consistent behavior of linear shear stress increase followed by gradual yield (Figure 2). After the shear load cycles we observe a period of stable sliding followed by emergent, quasi-periodic unstable slow-slip (Figure 2A. The stick-slip events are laboratory analogs of earthquakes. The labquakes are slow and complex initially, and reach a steady-state that is dictated by K and Kc. Samples typically reached peak friction at shear strains ranging from 7 - 9. After the slide-hold-slide test at 10 mm, sliding transitions from stable motion to quasi-unstable motion with small-amplitude oscillations that grow over 10 – 20 slip cycles (Figure 2B).

A separate suite of experiments were used to measure permeability evolution as a function of strain. Permeability evolved from 10^{-17} to 10^{-19} m^2 (see Supplementary Figure 2), with the greatest decrease occurring from 0 - 10 shear strain. Once the fault reached steady-state friction, permeability changes were small (see Supplementary Figure 2).

3.1 Lab earthquake measurements

For each slip event, we measured the co-seismic and inter-seismic periods using the maximum and minimum shear stress to define the beginning and end of failure. (Figure 2C, see Supplementary Figure 4). Stress drop was measured as the difference between the maximum shear stress before failure and the minimum shear stress after slip. Stress drops ranged from 0.01 to 0.65 MPa. Slip velocity was calculated using a 0.1 µm displacement-based moving window of the on-fault displacement. Peak slip velocities ranged from just above the background loading rate (10 µm/s) for slow events to 1100 µm/s for the fastest events. Slip event durations ranged from 0.3 to 7 s. Shear loading stiffness K was measured from (1) unloading/reloading cycles and (2) a linear fit to the shear stress curves during the locked (linear elastic) section of the seismic cycle (see Supplementary Figure 3).

3.2 Lab earthquakes with finite pore pressure

Experiments show a consistent pattern of stable sliding that transitions to stick-slip behavior and lab earthquakes after shear strains of 12 to 14 (Figure 3). The suite of experiments shows minor differences in frictional strength and strain weakening behavior (see Supplementary Figure 5), with peak friction ranging from 0.54 to 0.7. The transition from stable sliding to quasi-periodic slow-slip occurs at lower shear strains (11 – 13) for higher P_p (Figure 3). Despite the effect of P_p on stick-slip initiation, there is

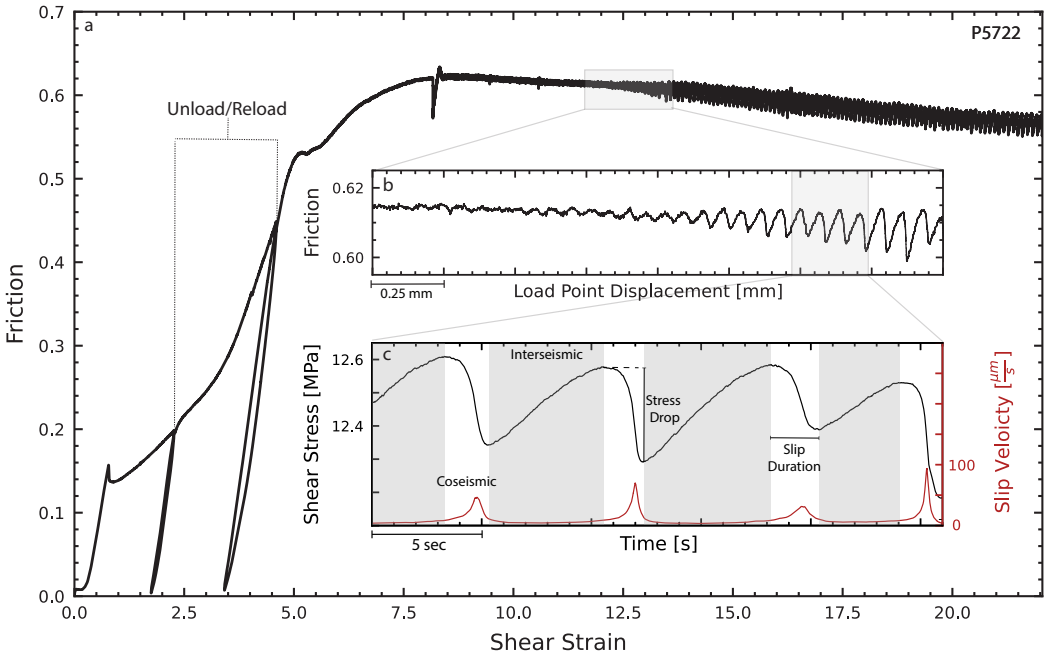

Figure 2. Data for one complete experiment showing fault zone shear stress and shear strain derived from shear displacement and fault thickness. (A) Steady-state friction was reached by shear strains of 7-9. (B) The transitions from stable sliding to slow periodic stick-slips occurred over a small displacement range and 10 - 20 seismic cycles. (C) For each stick-slip event, the co- and inter-seismic periods were defined via the shear stress. We measure stress drop, slip duration and slip velocity for each event. Shear loading stiffness was measured from the friction displacement curve during the locked stage of each event (see Supplementary Figure 3).

no clear correlation with the rate at which events reach a steady limit-cycle of labquake failure events, which we define as $< 10\%$ change in stress drop over a few mm of slip. We assume that steady-state labquake repeat times and stress drops are the result of reaching a steady fault zone shear fabric.

The transition from stable sliding to quasi-periodic slow-slip under fluid saturated conditions is quite similar to that observed in previous works without pore fluids (Scuderi et al., 2017; Leeman et al., 2016; Shreedharan et al., 2020). This stage typically has small amplitude modulations in shear stress of 10s of kPa and slip velocity just above background loading velocity. Periods of stable sliding and oscillatory modulation generally occur over the same shear displacement length scales (Figure 3A). There is no apparent correlation between the number of small amplitude modulations and when the fault transitions from stable sliding to quasi-periodic slow-slip. The transition from stable to unstable slip occurs during a period of small amplitude oscillations, and while the interseismic period remains near-constant the stress drop magnitude increases over 20 - 50 events before a steady-state stick-slip cycle is achieved. Over this range, labquake cycles have stress drops <0.2 MPa and slip velocities <100 µm/s. The co-seismic slip duration scales inversely with peak fault slip velocity (Figure 3B). For the transitory stage between stable and unstable slip, we note that the onset of failure is often irregular and difficult to identify, which could explain the data scatter (Figure 3C). As slip events become larger in magnitude and faster the fault creep rate during the interseismic period decreases systematically (see Supplementary Figure 6), matching previous works on the

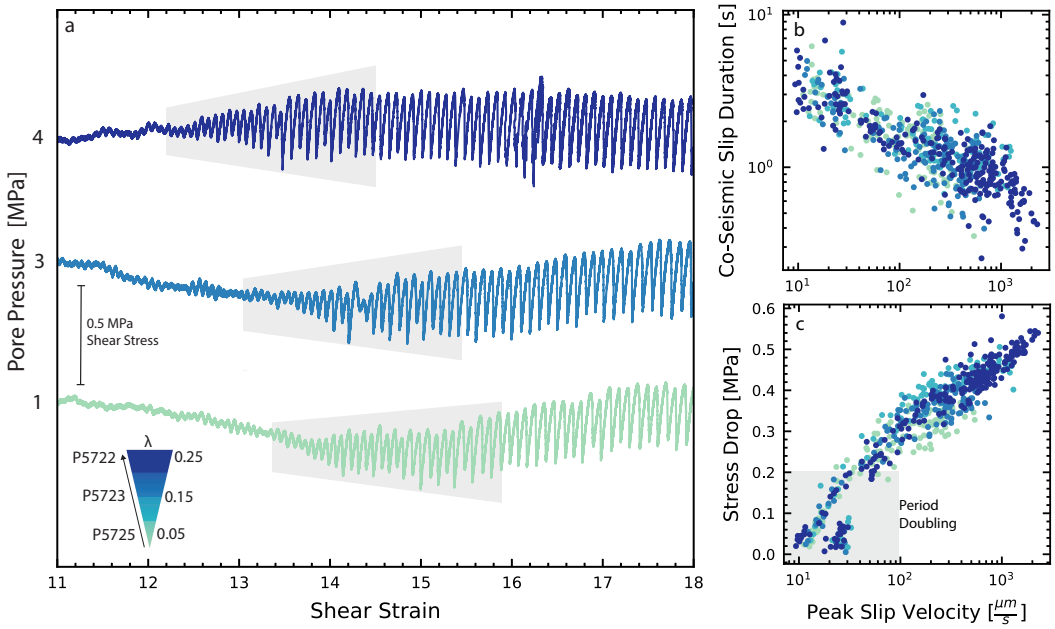

Figure 3. (a) Stick-slip event characteristics for experiments at 3 different pore pressures. Shear stress is plotted vs. shear strain during the transition from stable to unstable slip. The transition from small instabilities to quasi-periodic labquakes occurs over a few slip cycles (grey boxes). Panels (b) and (c) show event data for shear strains from 12 to 20 for our complete data set. Stick-slip events evolve from slow to fast, with a log-linear relationship between stress drop and slip velocity. Larger events, with bigger stress drops, reach peak fault slip velocity >1 mm/s with the largest stress drops and corresponding fastest events occurring at the highest λ values. Note the clear trend between co-seismic slip duration and stress drop.

relationship between stress drop and creep rate (Shreedharan et al., 2023). In addition, the co-seismic slip duration decreases during this stage. While friction reaches a quasi-steady state by shear strains of about 15, labquake stress drops continue to grow, going from 0.2 to 0.6 MPa with peak slip velocities going from 100 to 1100 µm/s.

3.3 Effect of loading stiffness on fault stability

For our apparatus, the transition from stable to unstable motion occurs when loading stiffness K is $\approx$ 0.015 MPa/µm (Leeman et al., 2015, 2016; Scuderi et al., 2016; Shreedharan et al., 2020). The effective stiffness increases initially upon loading as the fault zone compacts but then does not change appreciably after steady-state friction is reached. The onset of slow, quasi-periodic labquakes occurs at a low value of K and evolves over a shear strain of 5 –8 (Figure 4). This initial stage hosts complex slip behaviors including period doubling. Once steady-state stick-slip is achieved, K then increases at a much slower rate. Consistent with previous work, lower values of K produce larger events with bigger stress drop and higher slip velocity (Leeman et al., 2016; Rudolf et al., 2021). Event sizes and magnitudes continue to evolve as a function of strain, with more dynamic events occurring at progressively higher shear strains (Scuderi et al., 2017, 2020).

The stability transition occurs when K becomes $< K_c$, and we observe that both K and K_c evolve with shear strain. We present two estimates for the K_c envelope (Fig-

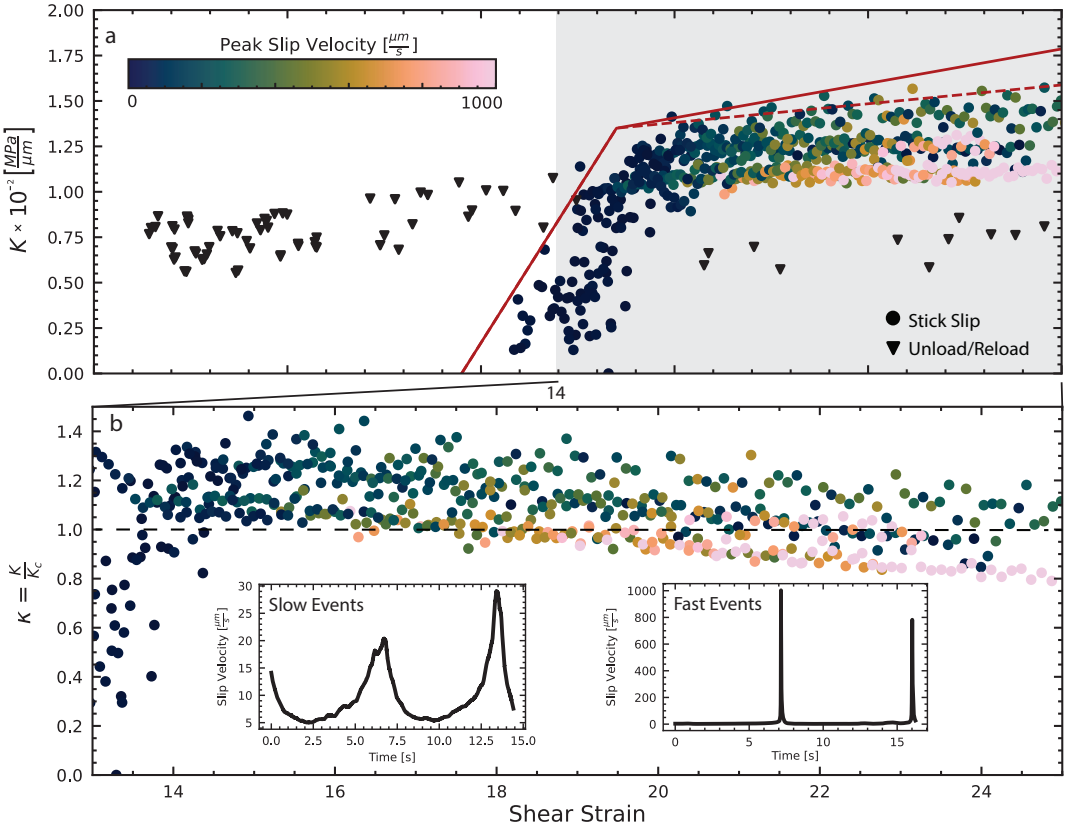

Figure 4. Loading stiffness K measured from experiments at 20 MPa σ_n' and P_p from 1 - 4 MPa (Supplement Table). (a). Data points show K values measured from unload-reload cycles and stick-slip. Lines show the evolution of K_c with shear strain; the solid line is the preferred model, dashed line shows an alternative model. Note that the transition from stable to unstable slip occurs at a shear strain of ≈ 14 (see also Fig. 1). (b) Zoom of the shaded portion of Panel A showing stick-slip evolution from slow to fast slip events, as predicted by theory when data fall below the dashed line showing $\kappa = 1$. Insets shows detail of slip velocity history during slow and fast events at shear strain of 15 and 22, respectively.

ure 4A). Both thresholds are determined from RSF parameters and a theoretical envelope based on stress dependence of frictional stability (Leeman et al., 2016; Scuderi et al., 2016). The first (dashed line) assumes minimal rheological evolution, such that K_c is roughly constant with shear and small changes in K are the cause of changes in event size (Gu et al., 1984; Leeman et al., 2016). Conversely, the second (solid line) shows a small evolution of K_c, consistent with lab data (Scuderi et al., 2017). The solid line accounts for small changes in frictional properties and their impact on instability. Because σ_n' is constant, K remains nearly constant throughout the experiment, changing only during initial shear when the fault zone compacts and stiffens. Such changes in the effective loading stiffness with strain are linked to densification and shear fabric development. However, increases in K_c with strain typically outpace changes in K. Therefore, once the critical stiffness ratio is reached, with ($\kappa = K/K_c \approx 1$), the evolution of event magnitude is primarily modulated *via* the rheological weakening rate K_c. We find that slow events correspond to κ values from 1.4 - 1.1, whereas faster, more dynamic events typ-

ically have κ below 1. The relation between κ and shear strain outpaces the effects of λ, such that all experiments follow a similar evolution from slow to fast regardless of P_p.

4 Discussion

P_p can affect the mode of frictional sliding *via* σ'_n and/or fluid drainage state as controlled by permeability and the rate of shearing rate and porosity change. The stability transition from stable to unstable sliding depends on σ'_n and P_p. Thus, changes in P_p could produce a change in stability by reducing the fault stress, which in isolation would tend to promote slow-slip and stable sliding. Another possibility is that quasi-dynamic changes in fault zone porosity could produce dilatant strengthening or, the opposite, weakening *via* fluid pressurization (Segall & Rice, 2006; Segall et al., 2010; Brantut, 2020). Our experiments test the assumption that pore fluid pressure alone is the driving mechanism for complex modes of fault slip. We explore how slow-slip can occur under finite P_p, even in cases where dilatancy strengthening is negligible, highlighting that it depends not only on the presence of pore fluids - but also on the magnitude of pore pressure and complexity of fluid pathways.

4.1 The effect of fluid pressure on lab earthqukes

Our results demonstrate that the stability transition from stable to unstable motion occurs gradually (Figure 2A) followed by evolution from slow and complex slip events to steady, quasi-periodic labquakes over 10 - 20 lab seismic cycles (Figure 3A). Instabilities nucleate at somewhat lower shear strain for higher λ, but with negligible effect on labquake stress drop or recurrence interval. For our range of P_p values the effective loading stiffness K is the same and we see similar behaviors, indicating that P_p has a minor effect on slip behavior (Figure 4A).

Importantly, our results indicate that under constant pressure conditions at low P_p, there is minimal effect on labquake initiation and evolution. We measured pore-pressure near the fault surface but not directly on it, which allows the possibility that dilational mechanisms existed but were potentially masked by measurement volume effects (Brantut, 2020). While we cannot rule this out completely, we note that our results are consistent with previous work using similar materials and absent of fluids (Leeman et al., 2016; Scuderi et al., 2016). These studies show that slow-slip and complex slip behaviors near the stability boundary are caused by velocity-dependent changes in the critical frictional weakening rate. With the consideration in mind, our results indicate that at low P_p conditions slow-slip is not produced by dilational mechanisms.

Previous works have documented the transition from stable to unstable stick-slip (Figure 2) as a function of stiffness (Leeman et al., 2016; Rudolf et al., 2021) by matching the effective loading stiffness K to the critical loading stiffness K_c, (Gu et al., 1984) such that $\kappa = K/K_c \leq 1$. The evolution of spontaneous stick-slips is widely agreed to depend on shear fabric evolution (Scuderi et al., 2017, 2020; Bedford & Faulkner, 2021) - where the RSF parameters continue to evolve such that K_c outpaces any increase in K sample compaction and geometric thinning of gouge.

Our results indicate that regardless of pore pressure, instabilities nucleate in the same envelope of K_c as previous studies (Leeman et al., 2016; Scuderi et al., 2017). This suggests that dilatant volume changes are minor and occur under drained fluid conditions. Importantly, we find that stick-slip magnitude increases as a function of shear strain (Figure 4A). The strain-dependent evolution of K_c has two mechanisms: (1) the dashed line assumes K is the driving mechanism for instabilities, where once the material reaches steady-state sliding, events should not change, or (2) the solid line suggests that shear strain sensitive processes, such as grain size reduction (Niemeijer et al., 2009, 2010; Collettini et al., 2011; Bedford & Faulkner, 2021), dictate how and when a fault will nucle-

ate laboratory stick-slip cycles. We posit that at constant stress conditions, when volumetric changes, and thus P_p are sufficiently small, shear fabric evolution is the driving mechanism promoting fault instability. We cannot rule out a role of P_p in natural fault systems, it seems likely that slow slip is caused by more than just pore fluids.

4.2 Fluid diffusion time and fault stability

Under fluid-saturated conditions, the stress dependence of frictional behavior and RSF parameters (a, b, D_c) depend on fault zone volume changes *via* dilation/compaction and the fluid diffusion time. Recent friction studies at higher pore pressure and also studies of rock fracture show that fault dilation can result in significant P_p transients (Brantut, 2020; Aben & Brantut, 2021). These experiments documented undrained conditions and local reduction of P_p. We evaluated the possibility that our experiments also involved undrained loading. We did this by comparing pore fluid volume changes with changes in layer thickness, following previous work (Samuelson et al., 2009). This comparison shows that our loading conditions were drained. The measured changes in layer thickness agree well with the pore volume measurements for our full range of conditions.

In other works, the evolution of fault zone permeability has been related to changes in porosity (Crawford et al., 2008; Faulkner et al., 2018) due to grain size reduction during shearing (Niemeijer et al., 2010; Collettini et al., 2011; Bedford & Faulkner, 2021). These work also suggest an increase in complexity of the fluid pathways due to shear fabric evolution perpendicular to the flow direction (Zhang et al., 1999). In this case, the characteristic drainage time due to the internal generation of pore fluid pressures is,

$$t = \frac{L^2 \eta * (\beta_p + \Phi \beta_w)}{2k} \tag{2}$$

where L is layer thickness, η is dynamic fluid viscosity, ϕ is porosity, k is permeability and β_p and β_w are the compressibility of the porous medium and fluid. For our experiments Equation 2 gives a fluid diffusion time of the order of 1 second, which is consistent with our measurements of porosity and layer thickness change (see Supplementary Figure 7). Thus, a shearing rate of 10 µm/s would sustain localized over-pressure or under-pressure – effectively weakening, or strengthening the fault. Within this framework, shear-induced changes in P_p are controlled by changes in fault volume and the duration of these effects would increase as permeability decreases. Therefore, at the same loading velocity, the permeability-shear strain evolution is the primary mechanism controlling P_p - slip responses. Critical to our study, is the minor impact of these local mechanisms on the bulk laboratory seismic cycle.

Importantly, our study demonstrates that at low P_p, despite the fault hosting instances of undrained fluid pressure, there is no resolvable effect on fault slip or stress drop. When fluid effects are important, fault weakening or strengthening is rate-controlled by fluid diffusion (Paola et al., 2007), the fault plane will experience periodic increased or decreased frictional strength based on the sense of porosity change (Sibson, 1986; Segall et al., 2010) - compactive or dilational. Our results demonstrate that across low P_p conditions, frictional processes alone are sufficiently explain stick-slip evolution. We postulate that not only high pore pressures, but significantly anisotropic permeability is required to elucidate the complex slip phenomena observed in nature.

5 Conclusion

We conducted well-controlled frictional shearing experiments to explore the origin of slow-slip and the frictional stability transition for conditions of finite pore pressure. We tested the hypothesis that slow slip is caused by changes in fluid pressure and dilatancy strengthening associated with undrained conditions. Our results show that this

hypothesis must be rejected. Instead, our data are consistent with the interpretation that the slow slip and complex modes of frictional sliding arise from variation of the rate of frictional weakening K_c as a function of slip velocity. Our data show that the transition from stable sliding to first quasi-periodic slow-slip and eventually elasto-dynamic fast labquakes is linked to changes in frictional properties that arise from shear fabric development. We conclude that elevated P_p and drainage-limited conditions, are required to activate dilational mechanisms controlling slip. We find that slow-slip and complex modes of fault motion can occur under finite P_p without dilatancy strengthening or undrained loading conditions.

Data Availability Statement

All data are available at https://doi.org/10.5281/zenodo.7734607.

Acknowledgments

We thank Steven Swavely for laboratory technical support and Drs. Srisharan Shreedharan, David (Chas) Bolton, Marco Scuderi, and Carolina Giorgetti for scientific support and discussions. This work was supported by US Department of Energy grants DE-SC0020512 and DE-EE0008763 and European Research Council Advance Grant 835,012 (TECTONIC).

References

Aben, F., & Brantut, N. (2021). Dilatancy stabilises shear failure in rock. *Earth and Planetary Science Letters*, *574*, 1–34. doi: 10.1016/j.epsl.2021.117174

Bedford, J. D., & Faulkner, D. R. (2021). The role of grain size and effective normal stress on localization and the frictional stability of simulated quartz gouge. *Geophysical Research Letters*, *48*(7), e2020GL092023.

Behr, W., & Bürgmann, R. (2021). What's down there? the structures, materials and environment of deep-seated slow slip and tremor. *Philosophical Transactions of the Royal Society A: Mathematical, Physical and Engineering Sciences*, *379*(2193). doi: 10.1098/rsta.2020.0218

Biot, M. (1941). General theory of three-dimensional consolidation. *Journal of Applied Physics*, *12*(2), 155-164. doi: 10.1063/1.1712886

Brantut, N. (2020). Dilatancy-induced fluid pressure drop during dynamic rupture: Direct experimental evidence and consequences for earthquake dynamics. *Earth and Planetary Science Letters*, *538*, 1–25. doi: 10.1016/j.epsl.2020.116179

Brantut, N., Sulem, J., & Schubnel, A. (2011). Effect of dehydration reactions on earthquake nucleation: Stable sliding, slow transients, and unstable slip. *Journal of Geophysical Research: Solid Earth*, *116*(B5). doi: 10.1029/2010JB007876

Bürgmann, R. (2018). The geophysics, geology and mechanics of slow fault slip. *Earth and Planetary Science Letters*, *495*, 112–134. doi: 10.1016/j.epsl.2018.04.062

Collettini, C., Niemeijer, A., Viti, C., Smith, S., & Marone, C. (2011). Fault structure, frictional properties and mixed-mode fault slip behavior. *Earth and Planetary Science Letters*, *311*(3-4), 316–327.

Condit, C., & French, M. (2022). Geologic evidence of lithostatic pore fluid pressures at the base of the subduction seismogenic zone. *Geophysical Research Letters*, *49*(12), e2022GL098862.

Crawford, B., Faulkner, D., & Rutter, E. (2008). Strength, porosity, and permeability development during hydrostatic and shear loading of synthetic quartz-clay fault gouge. *Journal of Geophysical Research: Solid Earth*, *113*(B3).

Dal Zilio, L., Lapusta, N., & Avouac, J.-P. (2020). Unraveling scaling properties of slow-slip events. *Geophysical Research Letters*, *47*(10), e2020GL087477.

Dieterich, J. (1979). Modeling of rock friction 1. experimental results and constitutive equations. *Journal of Geophysical Research: Solid Earth*, *84*(B5), 2161–2168. doi: 10.1029/JB084iB05p02161

Ellsworth, W. (2013). Injection-induced earthquakes. *Science*, *341*(6142), 1225942. doi: 10.1126/science.1225942

Faulkner, D., & Rutter, E. (2001). Can the maintenance of overpressured fluids in large strike-slip fault zones explain their apparent weakness? *Geology*, *29*(6), 503–506.

Faulkner, D., Sanchez-Roa, C., Boulton, C., & Den Hartog, S. (2018). Pore fluid pressure development in compacting fault gouge in theory, experiments, and nature. *Journal of Geophysical Research: Solid Earth*, *123*(1), 226–241.

Gu, J., Rice, J., Ruina, A., & Tse, S. (1984). Slip motion and stability of a single degree of freedom elastic system with rate and state dependent friction. *Journal of the Mechanics and Physics of Solids*, *32*(3), 167–196. doi: 10.1016/0022-5096(84)90007-3

Hubbert, K., & Rubey, W. (1959). Role of fluid pressure in mechanics of overthrust faulting: I. mechanics of fluid-filled porous solids and its application to overthrust faulting. *GSA Bulletin*, *70*(2), 115-166. doi: 10.1130/0016-7606(1959)70[115:ROFPIM]2.0.CO;2

Ikari, M., Saffer, D., & Marone, C. (2009). Frictional and hydrologic properties of clay-rich fault gouge. *Journal of Geophysical Research: Solid Earth*, *114*(B5). doi: 10.1029/2008JB006089

Ji, Y., Hofmann, H., Rutter, E., & Zang, A. (2022). Transition from slow to fast injection-induced slip of an experimental fault in granite promoted by elevated temperature. *Geophysical Research Letters*, *49*(23), e2022GL101212.

Kenigsberg, A., Rivière, J., Marone, C., & Saffer, D. (2020). Evolution of elastic and mechanical properties during fault shear: The roles of clay content, fabric development, and porosity. *Journal of Geophysical Research: Solid Earth*, *125*(3), 1–16. doi: 10.1029/2019JB018612

Leeman, J., Saffer, D., Scuderi, M., & Marone, C. (2016). Laboratory observations of slow earthquakes and the spectrum of tectonic fault slip modes. *Nature Communications*, *7*, 1–6. doi: 10.1038/ncomms11104

Leeman, J., Scuderi, M., Marone, C., & Saffer, D. (2015). Stiffness evolution of granular layers and the origin of repetitive, slow, stick-slip frictional sliding. *Granular Matter*, *17*(4), 447–457. doi: 10.1007/s10035-015-0565-1

Marone, C. (1998). Laboratroy-derived friction laws and their application to seismic faulting. *Annual Review of Earth and Planetary Sciences*, *26*(1), 643-696. doi: 10.1146/annurev.earth.26.1.643

Marone, C., Raleigh, C., & Scholz, C. (1990). Frictional behavior and constitutive modeling of simulated fault gouge. *Journal of Geophysical Research*, *95*, 7007-7025. doi: 10.1029/JB095iB05p07007

Niemeijer, A., Elsworth, D., & Marone, C. (2009). Significant effect of grain size distribution on compaction rates in granular aggregates. *Earth and Planetary Science Letters*, *284*(3-4), 386–391.

Niemeijer, A., Marone, C., & Elsworth, D. (2010). Frictional strength and strain weakening in simulated fault gouge: Competition between geometrical weakening and chemical strengthening. *Journal of Geophysical Research: Solid Earth*, *115*(10), 1–16. doi: 10.1029/2009JB000838

Paola, N. D., Collettini, C., Trippetta, F., Barchi, M. R., & Minelli, G. (2007). A mechanical model for complex fault patterns induced by evaporite dehydration and cyclic changes in fluid pressure. *Journal of Structural Geology*, *29*(10), 1573-1584. Retrieved from `https://www.sciencedirect.com/science/article/pii/S0191814107001411` doi: https://doi.org/10.1016/

j.jsg.2007.07.015

Proctor, B., Lockner, D., Kilgore, B., Mitchell, T., & Beeler, N. (2020). Direct evidence for fluid pressure, dilatancy, and compaction affecting slip in isolated faults. *Geophysical Research Letters*, *47*(16). doi: 10.1029/2019GL086767

Rice, J. (2006). Heating and weakening of faults during earthquake slip. *Journal of Geophysical Research: Solid Earth*, *111*(B5). doi: 10.1029/2005JB004006

Rudolf, M., Rosenau, M., & Oncken, O. (2021). The spectrum of slip behaviors of a granular fault gouge analogue governed by rate and state friction. *Geochemistry, Geophysics, Geosystems*, *22*(12), e2021GC009825.

Ruina, A. (1983). *Slip instability and state variable friction laws* (Vol. 88) (No. B12). doi: 10.1029/JB088iB12p10359

Sacks, I. S., Linde, A. T., Suyehiro, S., & Snoke, J. A. (1978). Slow earthquakes and stress redistribution. *Nature*, *275*(5681), 599–602.

Samuelson, J., Elsworth, D., & Marone, C. (2009). Shear-induced dilatancy of fluid-saturated faults: Experiment and theory. *Journal of Geophysical Research: Solid Earth*, *114*(12), 1–15. doi: 10.1029/2008JB006273

Scholz, C., Molnar, P., & Johnson, T. (1972). Detailed studies of frictional sliding of granite and implications for the earthquake mechanism. *Journal of geophysical research*, *77*(32), 6392–6406.

Scuderi, M., Collettini, C., Vitti, C., Tinti, E., & Marone, C. (2017). Evolution of shear fabric in granular fault gouge from stable sliding to stick slip and implications for fault slip mode. *Geology*, *45*(8), 731-734. doi: 10.1130/G39033.1

Scuderi, M., Marone, C., Tinti, E., Di Stefano, G., & Collettini, C. (2016). Precursory changes in seismic velocity for the spectrum of earthquake failure modes. *Nature Geoscience*, *9*(9), 695–700. doi: 10.1038/ngeo2775

Scuderi, M., Tinti, E., Cocco, M., & Collettini, C. (2020). The role of shear fabric in controlling breakdown processes during laboratory slow-slip events. *Journal of Geophysical Research: Solid Earth*, *125*(11), e2020JB020405.

Segall, P., & Rice, J. (2006). Does shear heating of pore fluid contribute to earthquake nucleation? *Journal of Geophysical Research: Solid Earth*, *111*(B9).

Segall, P., Rubin, A., Bradley, A., & Rice, J. (2010). Dilatant strengthening as a mechanism for slow slip events. *Journal of Geophysical Research: Solid Earth*, *115*(12), 1–37. doi: 10.1029/2010JB007449

Shreedharan, S., Bolton, D., Rivière, J., & Marone, C. (2020). Preseismic fault creep and elastic wave amplitude precursors scale with lab earthquake magnitude for the continuum of tectonic failure modes. *Geophysical Research Letters*, *47*(8), 1–10. doi: 10.1029/2020GL086986

Shreedharan, S., Saffer, D., Wallace, L., & Williams, C. (2023). Ultralow frictional healing explains recurring slow slip events. *Science*, *379*(6633), 712-717. Retrieved from `https://www.science.org/doi/abs/10.1126/science.adf4930` doi: 10.1126/science.adf4930

Sibson, R. (1986). Earthquakes and rock deformation in crustal fault zones. *Annual Review of Earth and Planetary Sciences*, *14*(1), 149-175. doi: 10.1146/annurev.ea.14.050186.001053

Wibberley, C. (2002). Hydraulic diffusivity of fault gouge zones and implications for thermal pressurization during seismic slip. *Earth, Planets and Space*, *54*(11), 1153–1171. doi: 10.1186/BF03353317

Williams, R. (2019). Coseismic boiling cannot seal faults: Implications for the seismic cycle. *Geology*, *47*(5), 461-464. doi: 10.1130/G45936.1

Zhang, S., Tullis, T., & Scruggs, V. (1999). Permeability anisotropy and pressure dependency of permeability in experimentally sheared gouge materials. *Journal of structural geology*, *21*(7), 795–806.

Figure1.

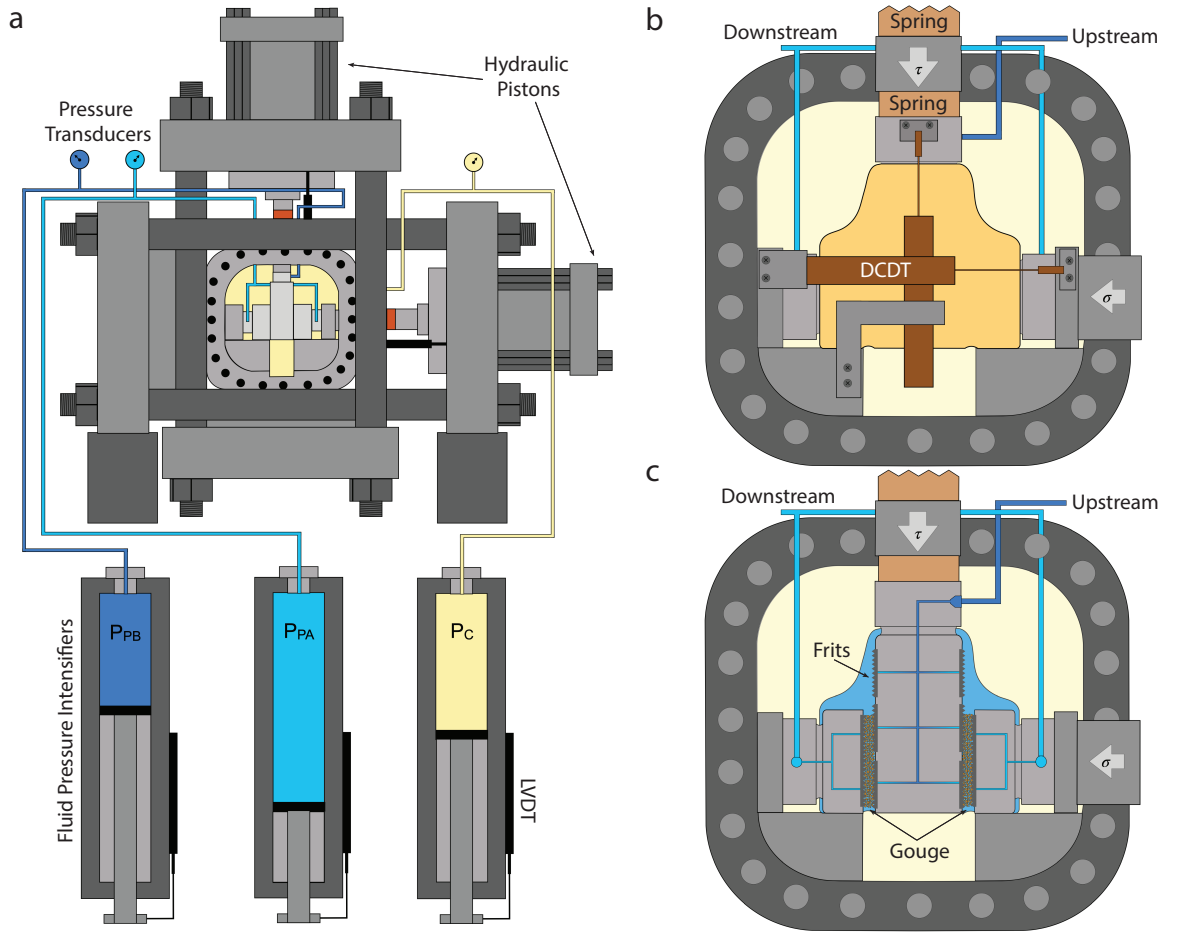
a
Hydraulic Pistons
Pressure Transducers
Fluid Pressure Intensifiers
P_{PB}
P_{PA}
P_C
LVDT
b
Downstream
Spring
Upstream
τ
Spring
DCDT
σ
c
Downstream
Upstream
τ
Frits
σ
Gouge

Figure2.

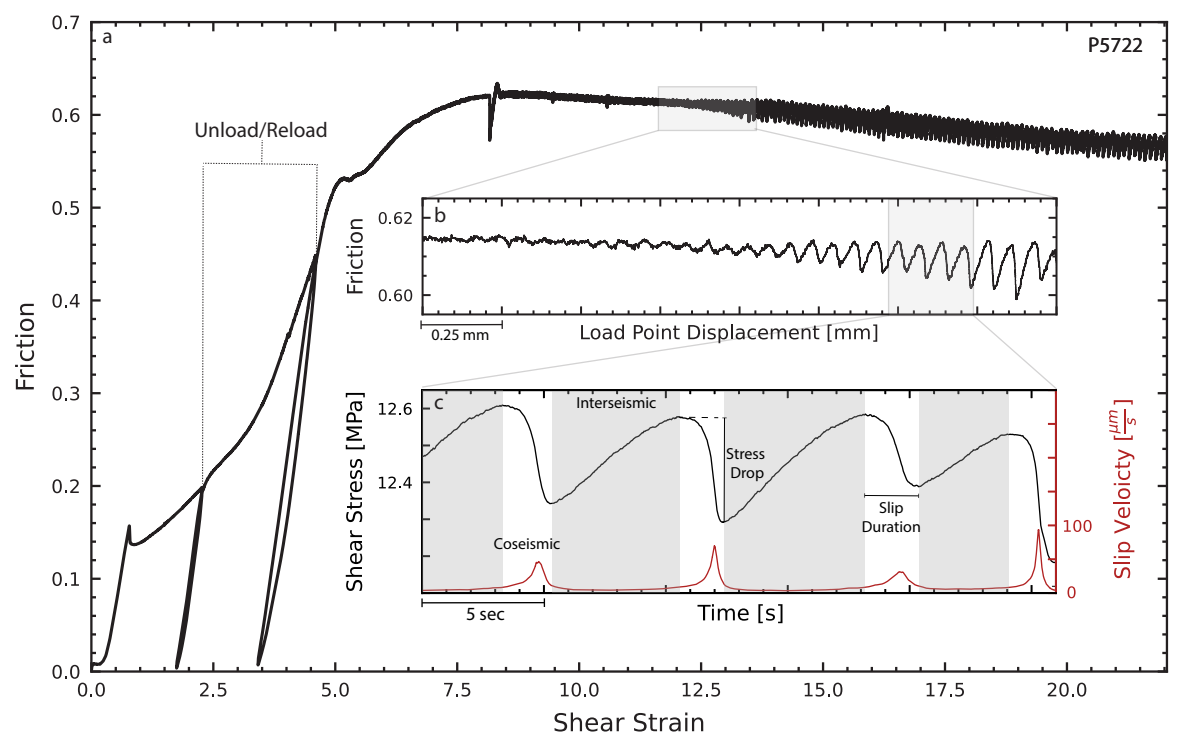
a
P5722
Unload/Reload
Friction
Shear Strain
0.0
0.1
0.2
0.3
0.4
0.5
0.6
0.7
0.0
2.5
5.0
7.5
10.0
12.5
15.0
17.5
20.0
b
Friction
0.62
0.60
0.25 mm
Load Point Displacement [mm]
c
Shear Stress [MPa]
12.6
12.4
Interseismic
Stress Drop
Slip Duration
Coseismic
5 sec
Time [s]
Slip Velocity [$\frac{\mu m}{s}$]
100
0

Figure3.

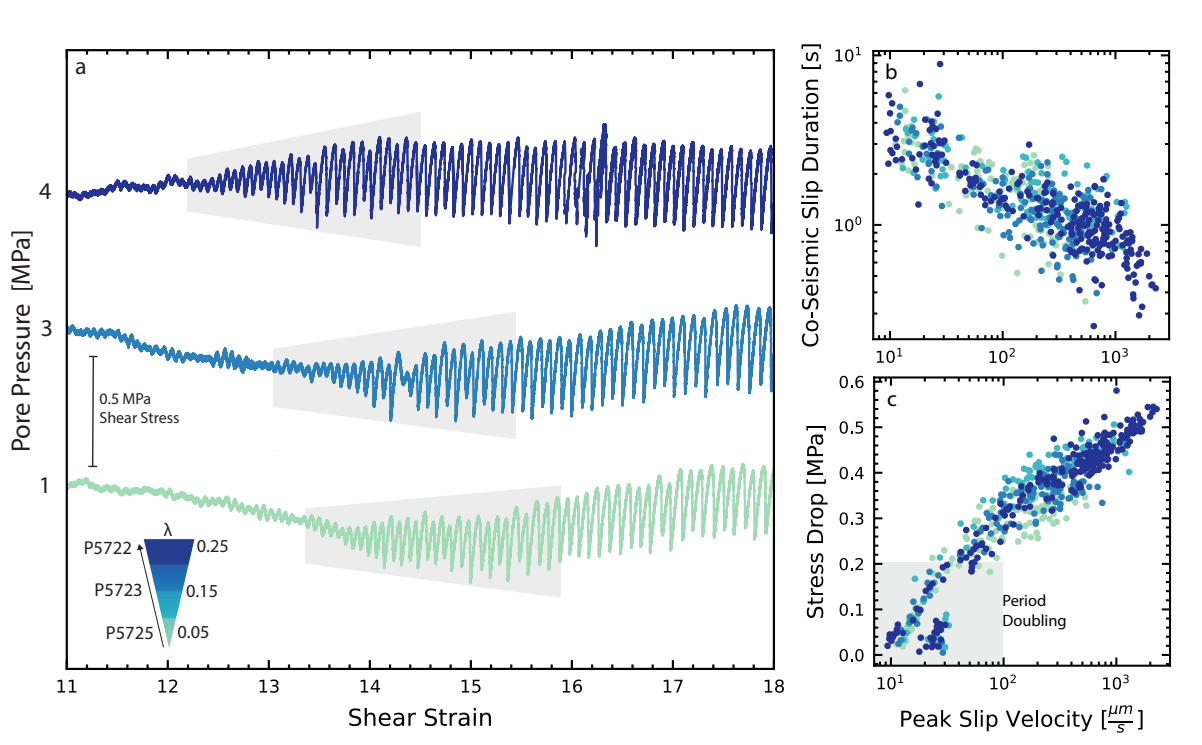
a
b
c
Pore Pressure [MPa]
4
3
1
0.5 MPa
Shear Stress
λ
P5722
0.25
P5723
0.15
P5725
0.05
11
12
13
14
15
16
17
18
Shear Strain
Co-Seismic Slip Duration [s]
10^1
10^0
10^1
10^2
10^3
Stress Drop [MPa]
0.6
0.5
0.4
0.3
0.2
0.1
0.0
Period
Doubling
10^1
10^2
10^3
Peak Slip Velocity [$\frac{\mu m}{s}$]

Figure4.

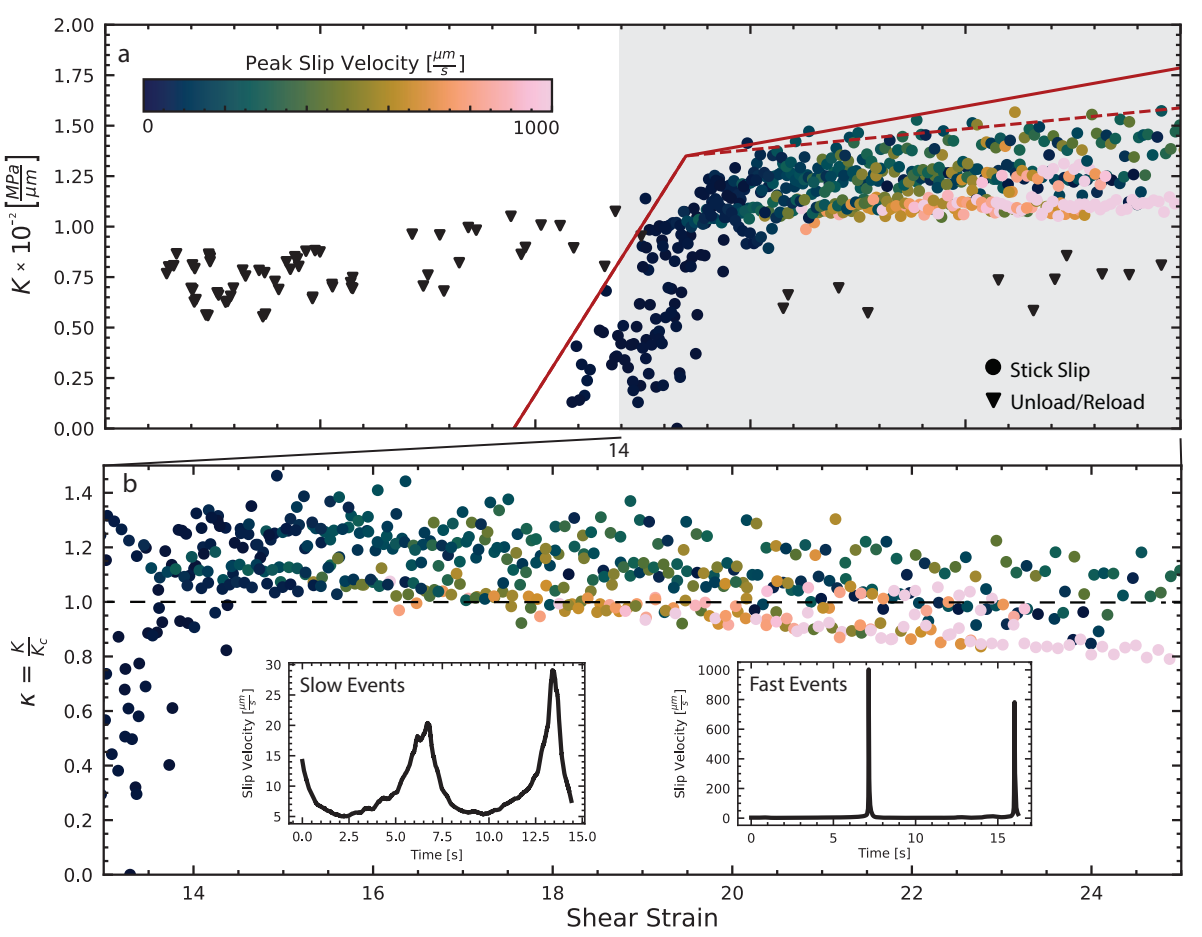
a
Peak Slip Velocity [$\frac{\mu m}{s}$]
0
1000
$K \times 10^{-2}$ [$\frac{MPa}{\mu m}$]
Stick Slip
Unload/Reload
14
b
$\kappa = \frac{K}{K_c}$
Slow Events
Slip Velocity [$\frac{\mu m}{s}$]
Time [s]
Fast Events
Slip Velocity [$\frac{\mu m}{s}$]
Time [s]
Shear Strain

Supporting Information for The Stability Transition from Stable to Unstable Frictional Slip with Finite Pore Pressure

R. Affinito[1], C. Wood[1], S. Marty[1], D. Elsworth[1,3], C. Marone[1,2]

[1]Department of Geoscience, Pennsylvania State University

[2]Dipartimento di Scienze della Terra, La Sapienza Università di Roma

[3]Deptartment of Energy and Mineral Engineering, EMS Energy Institute, and G3 Center, Pennsylvania State University

[1]Department of Geosciences, 503 Deike Building, University Park, PA 16802 USA

[2]EMS Energy Institute, Penn State University, C-211 Coal Utilization Laboratory, University Park, PA 16802 USA

[3]Department of Earth Sciences, La Sapienza University of Rome, P.le Aldo Moro, 5 - 00185 Rome, Italy

Corresponding author: R. A. Affinito, Department of Geosciences, 503 Deike Building, University Park, PA 16802 USA (affinito@psu.edu)

March 14, 2023, 9:05pm

Additional Supporting Information (Files uploaded separately)

1. Supporting datasets uploaded to the following:

Contents of this file

Introduction

The following information was collected alongside the data presented in the manuscript. Reported below is an overview of the experiments conducted, calibrations, and measurements that support the recorded findings. No known anomalies are recorded within the data. Any and all information can be provided upon request.

Supplemental Table

ID	σ_n **[MPa]**	P_p **[MPa]**	P_c **[MPa]**	λ	**Loading Velocity** $[\frac{\mu m}{s}]$	**Slip Type**
P5609	15	0	0	0	1,3,10	Stable
P5610	17	5	10	0.2	10	Unstable
P5611	18	5	8	0.25	10	Unstable
P5612	20	4	5	0.22	1,3,10	Stable
P5613	15	5	10	0.2	10	Unstable
p5633	18	1	5	0.05	10	Unstable
P5637	19	2	5	0.09	10	Unstable
P5638	19	2	5	0.09	10	Unstable
P5640	20	3	5	0.12	10	Unstable
P5661	21	4	5	0.2	10	Unstable
P5705	21	4	5	0.2	10	Unstable
P5722	21	4	5	0.2	10	Unstable
P5723	20	3	5	0.12	10	Unstable
P5724	19	2	5	0.09	10	Unstable
P5725	18	1	5	0.05	10	Unstable
P5804	21	4	5	0.2	3, 10, 30	Stable

Table S1. Experiment List

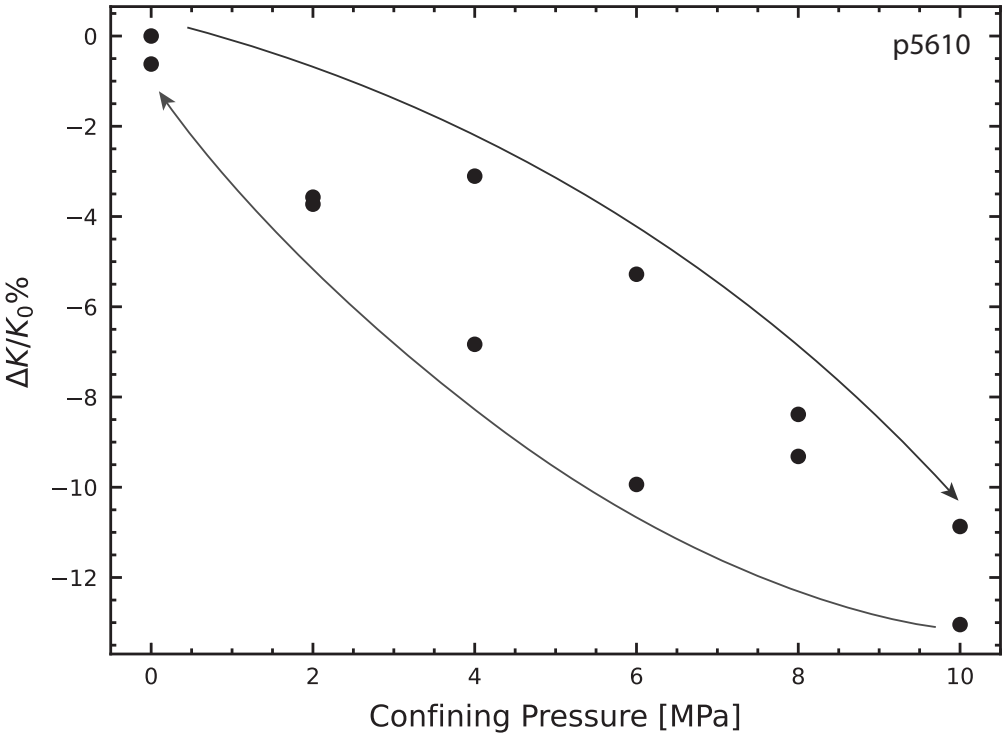

Figure S1. Measurements of the loading stiffness made from shear load/unload cycles at confining pressures from 0 to 10 MPa. These are effective stiffness values and include the acrylic spring inside the pressure vessel, the load frame and the fault zones. Note that the changes are roughly 1% per 1MPa of confining pressure. Experiments were done at 5 MPa confining pressure.

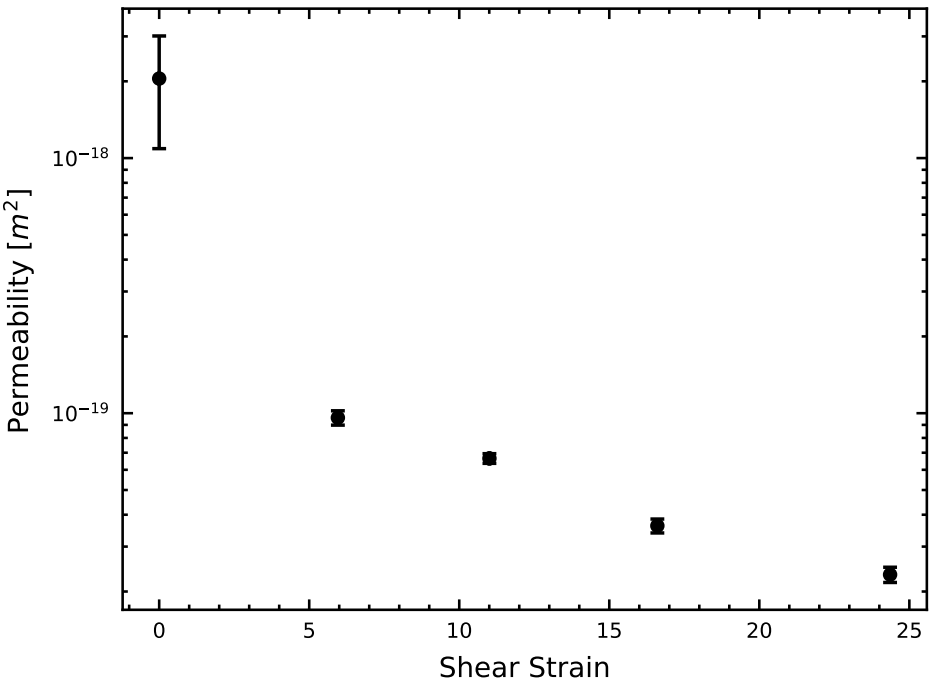

Figure S2. Permeability normal to the fault zones as a function of shear strain. The changes are largest during initial shear, for shear strains up to 10, when the fault zones are compacting. Error bars show the degree of variability from repeat measurements.

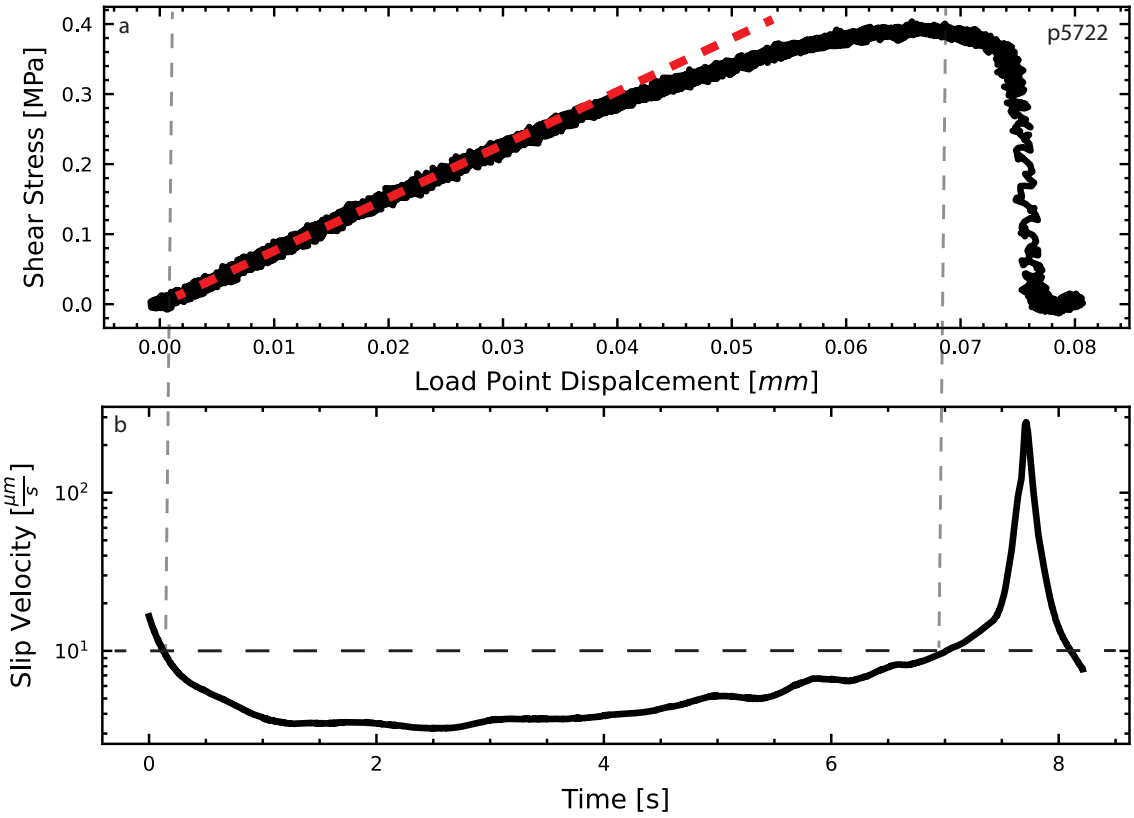

Figure S3. Example of the stiffness measurement technique. Part of a lab seismic cycle is shown as shear stress versus load point displacement (a), and the corresponding fault slip velocity (b). The data window is chosen by where the event 'locks' (green dot - slip velocity drops below the background loading rate) and it extends to the unlocking stage (red dot - slip velocity surpasses the background loading rate). A linear fit is done from the green dot, until the standard deviation increases past a threshold (a). As such, the linear fit is weighted toward the section with the lowest fault creep velocity (b)

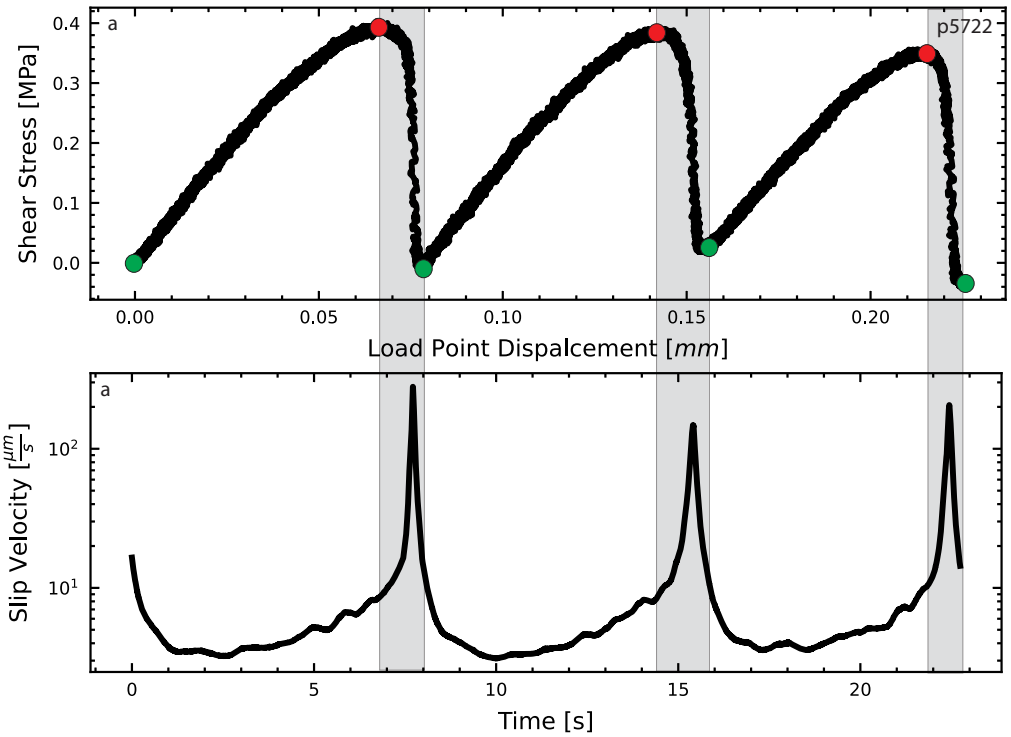

Figure S4. Example of stick-slip picking method. Three laboratory stick-slip cycles in shear stress as a function of load point displacement (a) and slip velocity as a function of time (b). For each event, the maximum shear stress (red dot), and the following minimum (green dot) are indexed. The maximum and minimum are used to define the co- and interseismic periods (co-seismic stages are outlined in grey). All experiments are indexed with the same method for consistency.

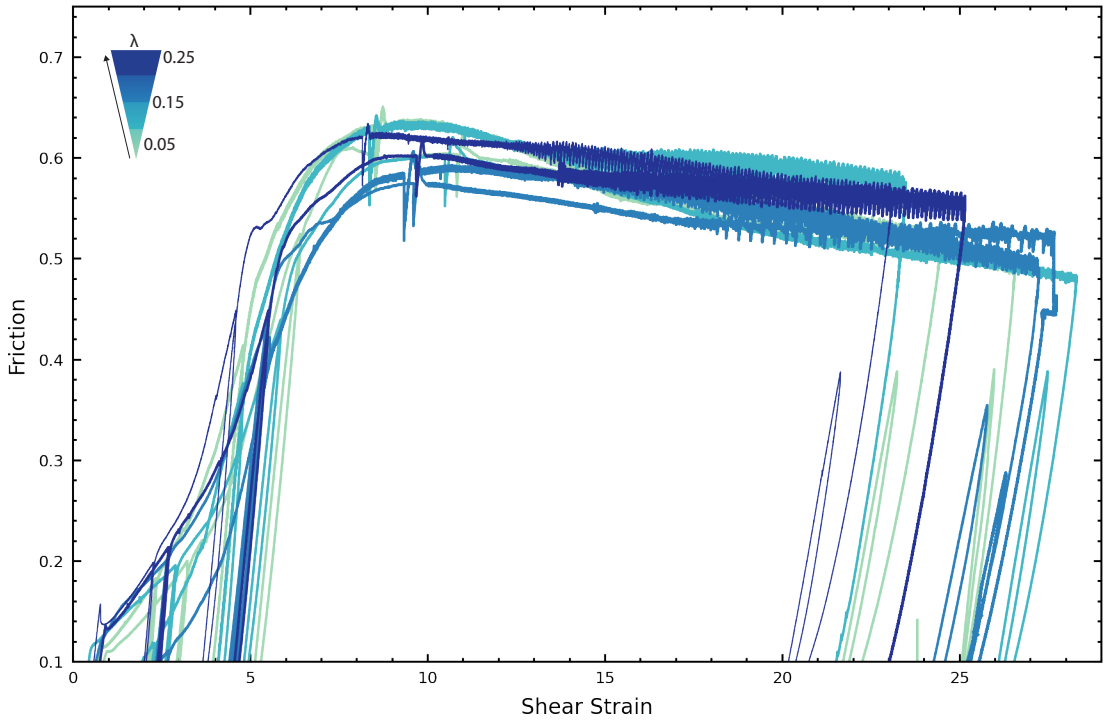

Figure S5. Friction versus shear strain plots for all stick-slip experiments outlined in Table 1. Peak friction varies between experiments based on the effective normal stress and compaction duration.

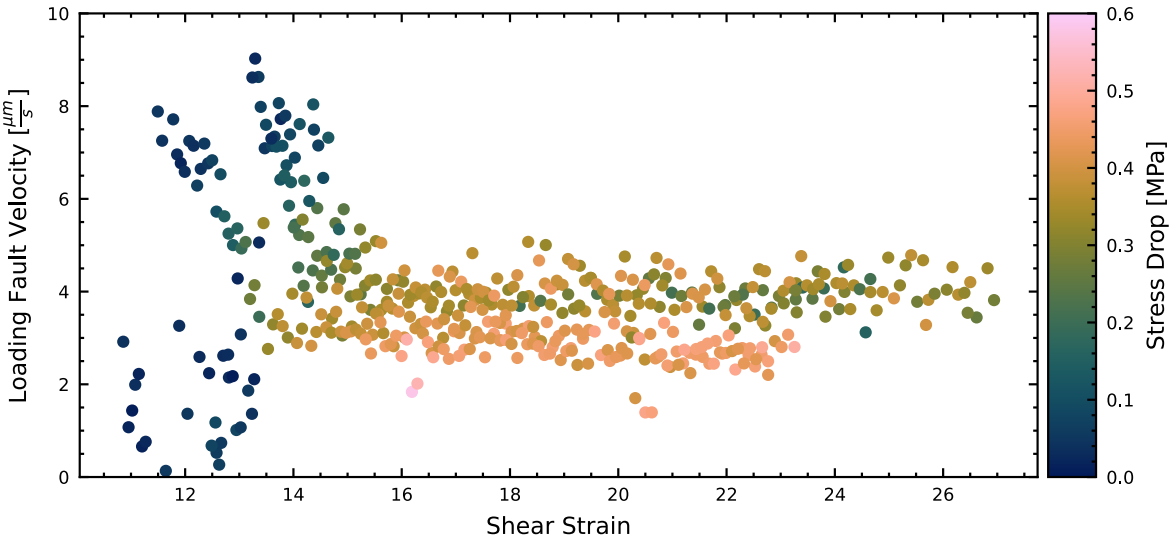

Figure S6. The loading fault creep velocity as a function of shear strain for all experiments. Fault loading creep velocities are measured using the minimum fault velocity during loading. Slower events correspond to low shear strains and stress drops of creep velocities near the background loading rate. Events that have higher shear strain and have greater stress drops are more locked.

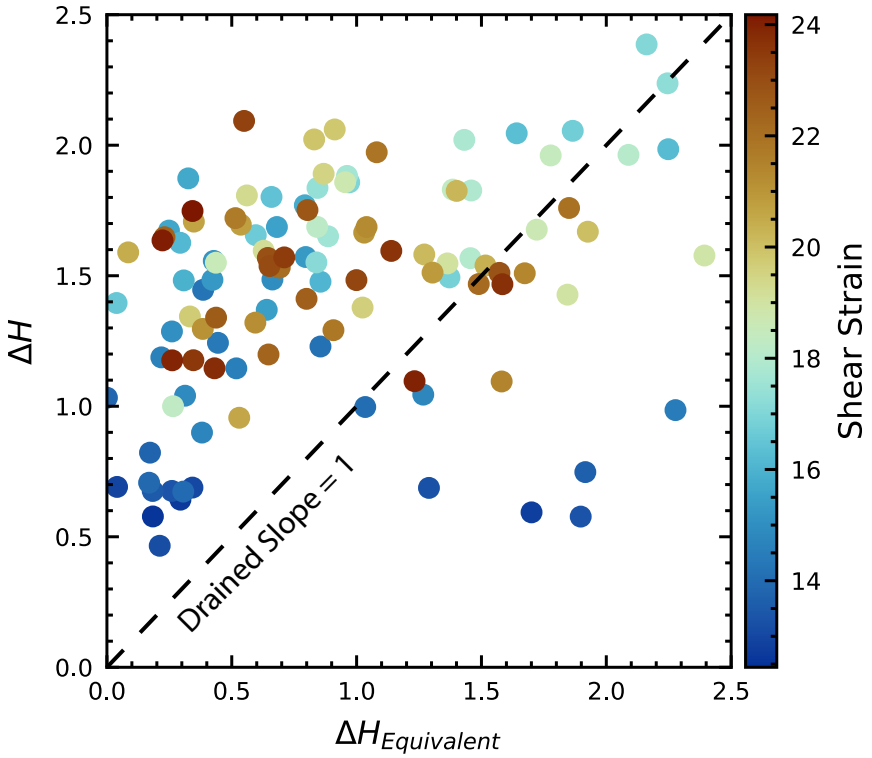

Figure S7. Measured changes in layer thickness (dilation corresponds to positive values of ΔH) vs. changes in layer thickness derived from pore volume measurements ΔV. The fault normal stress is constant so $\Delta V/V$ represents volume strain due to porosity changes and we determine $\Delta H_{Equivlaent}$ from volume strain. When the fault is fully drained these measurements should be equal and have a slope of 1. Our results indicate that the fault behaves predominantly undrained. At high shear strains there is some suggestion of undrained loading but the differences are small and decrease with the magnitude of ΔH, which would indicate drained conditions.

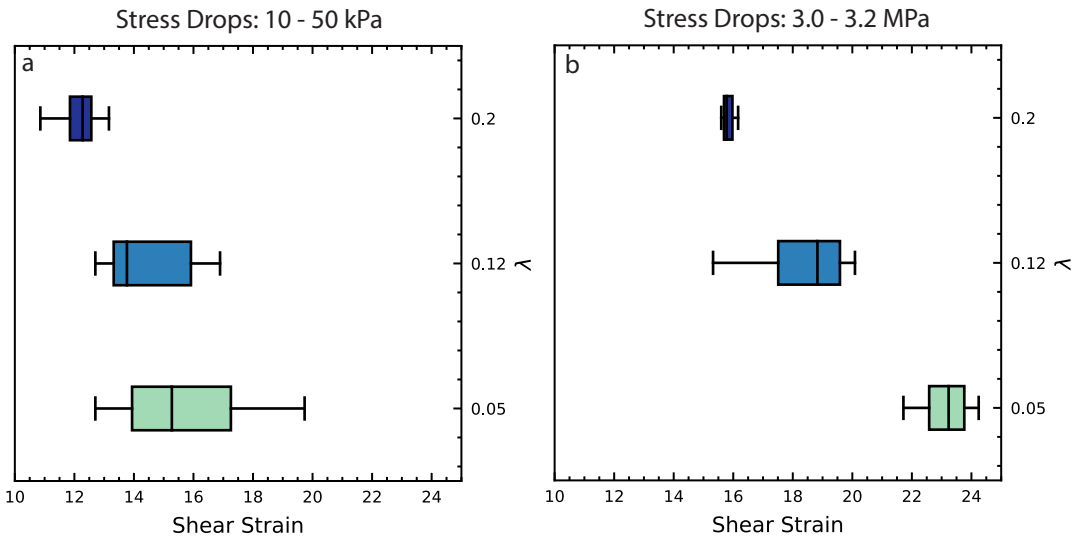

Figure S8. Box and whisker plots for stress drop as a function of strain for all experiments. The distribution of stress drops from 10 - 50kPa shown for each pore pressure condition (a). The distribution of stress drops from 0.3 - 0.32 MPa for each pore pressure condition. The onset of instabilities occurs at lower shear strains for high λ experiments.